*Exploration Geophysics (2005) **36**, 189–197*

The Total Field Magnetometric Resistivity(TFMMR) Method Part II: 2D resistivity inversion of data from the Flying Doctor Deposit, Broken Hill, Australia

Nader Fathianpour[1] **Graham Heinson**[2] **Antony White**[3]

Key Words: TFMMR, Marquardt-Levenberg inversion, Quasi-Newton approximation, Fréchet derivatives, Flying Doctor Deposit, Broken Hill

ABSTRACT

Total field magnetometric resistivity (TFMMR) is a high-resolution electrical technique that yields information on sub-surface resistivity. In a companion paper (Fathianpour et al., 2005, Part I) the basis of a 2.5D TFMMR finite-element modelling approach was developed for a point current source in an otherwise 2D resistivity structure. In this paper (Part II), we use the 2.5D forward modelling algorithm as the basis of a numerical inversion for 2D resistivity structure using a Marquardt-Levenberg algorithm. Application of a quasi-Newton updating formula for approximating the Fréchet derivatives in the course of inversion results in a fast and reliable routine. To overcome the problems of the effect of the geomagnetic field direction and dependency of TFMMR data on all three vector-components, field data are initially reduced to the pole. By doing this, we require only Fréchet derivatives for the vertical B_z anomalous magnetic field, and in the case of the 2D structures, B_z is the most sensitive component to vertical boundaries separating lateral changes in resistivity.

TFMMR data collected across the Flying Doctor Deposit, near Broken Hill in New South Wales, Australia are inverted for 2D resistivity structure. The inverse models show the presence of a conductive zone in the central part of the surveying area corresponding to the known mineralisation and the Globe Vauxhall Shear Zone. Depth resolution is limited, but we demonstrate that the method can resolve lateral boundaries.

INTRODUCTION

The basic principles applied to DC electrical methods can be developed to formulate the problem of inverting TFMMR data. In a companion paper (Fathianpour et al., 2005) it was shown theoretically that the anomalous magnetic field is a function of the resistivity contrasts between media with different resistivities. Consequently, the absolute values of the resistivities do not affect the shape or the magnitude of the anomalous field, which introduces an intrinsic non-uniqueness.

The other important aspect of inverting TFMMR data is the dependence on all three components of the anomalous magnetic field. Each component has a different sensitivity with respect to the model parameters, and therefore in the case of using gradient methods of optimisation the full inversion process of the original data becomes not only computationally intensive (slow convergence) but also unstable, particularly when close to the final solution. The other less important factor is the direction of the geomagnetic field that can significantly distort the shape of the TFMMR anomalous field.

In the case of inverting TFMMR data using gradient methods, we propose a pre-processing reduction of data to the pole to overcome the problems of the effect of the geomagnetic field direction and dependency of the TFMMR data on all three components. The TFMMR response is therefore just given by the anomalous B_z component. For 2D models, the vertical component is also the most sensitive component to the vertical structures.

In this paper, we outline the steps involved for numerical inversion of TFMMR data. Firstly, we develop the equations to calculate Fréchet derivatives for electric potentials and the B_z magnetic field components in the wavenumber domain, and hence the spatial domain. The numerical inversion method uses the Marquardt-Levenberg approach with a smoothness constraint, and quasi-Newton updating of the Jacobian matrix. Finally, we apply the inversion method to TFMMR data collected across the Flying Doctor Deposit, near Broken Hill.

FRÉCHET DERIVATIVES

A fundamental step in the solution of most non-linear inverse problems is to establish a relationship between model changes and forward modelled data (McGillivray and Oldenburg, 1990). Dependence of the data on changes in the model is given by a set of partial derivatives, or sensitivities, commonly known as Fréchet derivatives, that form elements of the Jacobian matrix **J**.

Consider a point source of current applied to a 2D resistivity structure $\rho(x, z)$ (or in terms of conductivity, $\sigma(x, z)$). The vertical component of the anomalous magnetic field $\bar{B}_z$ in the wavenumber domain is given by:

$$\bar{B}_z(x,k_y,z) = \frac{\mu_0}{2\pi}\int_0^\infty\int_{-\infty}^{\infty} k_y \frac{\partial\,\sigma(x',z')}{\partial\,x'}\bar{\phi}(x',k_y,z')\mathrm{K}_0(k_y r')\,dx'dz' \quad , (1)$$

(Fathianpour et al., 2005; equation (24)) in which

$$r' = \sqrt{(x-x')^2 + (z-z')^2} \quad , \qquad (2)$$

[1] *Department of Mining Engineering*
Isfahan University of Technology
Isfahan 84154, Iran
Phone: +98 311 391 5130
Facsimile: +98 311 391 2776
Email: fathian@cc.iut.ac.ir

[2] *Co-operative Research Centre*
for Landscapes Environment and Mineral Exploration
School of Earth and Environmental Sciences
University of Adelaide, Adelaide SA 5005, Australia

[3] *School of Chemistry, Physics and Earth Sciences*
Flinders University of South Australia
Bedford Park SA 5042, Australia

Manuscript received 6 August, 2004.
Revised manuscript received 13 April, 2005.

and k_y is a wavenumber in the *y*-direction. In equation (1), conductivity $\sigma(x, z)$ varies in the *x*- and *z*-directions, but is constant in the *y*-direction. The term $\phi(x',k_y,z')$ is the electric potential in the wavenumber domain, and K_0 is a zeroth-order Bessel function. Note that in equation (1), the $\bar{B}_z$ component depends only on the horizontal gradient of conductivity $\partial\sigma(x',z')/\partial x'$ and not on absolute values of conductivity. Thus, the TFMMR method has resolution only of lateral boundaries in conductivity, and little depth resolution.

The 2D model is parameterised by replacing the continuous conductivity distribution $\sigma(x, z)$ by a set of *M* individual blocks of constant conductivities that extend to infinity in the strike direction (*y*-direction) (McGillivray and Oldenburg, 1990):

$$\sigma(x,z)=\sum_{m=1}^{M}\sigma_m\psi_m(x,z), \tag{3}$$

where the basis function ψ_m is defined as:

$$\psi_m(x,z)=\begin{cases}1 & \text{for } \sigma(x,z)=\sigma_{\mathrm{m}}\\ 0 & \text{otherwise}\end{cases}. \tag{4}$$

Substituting equation (3) into equation (1) and differentiating with respect to σ_m yields:

$$\frac{\partial\bar{B}_z}{\partial\sigma_m}= \frac{\mu_0}{2\pi}\int_0^{\infty}\int_{-\infty}^{\infty}k_y\left[\frac{\partial\bar{\phi}}{\partial\sigma_m}\sum_{i=1}^{M}\sigma_m\cdot\frac{\partial\psi_m(x',z')}{\partial x'}+\bar{\phi}\,\delta(\sigma(x',z')-\sigma_m)\frac{\partial\psi_m(x',z')}{\partial x'}\right]\mathrm{K}_0(k_y r')\,\mathrm{d}x'\mathrm{d}z', \tag{5}$$

where

$$\delta(\sigma(x',z')-\sigma_m)=\begin{cases}1 & \text{when } \sigma(x',z')=\sigma_m\\ 0 & \text{otherwise}\end{cases}. \tag{6}$$

Evaluation of the TFMMR (B_z) magnetic field Fréchet derivatives in equation (5) is carried out in three steps:

1. Evaluate electric potential Fréchet derivatives $\partial\phi/\partial\sigma_m$ in the wavenumber domain for a range of wavenumbers k_y;
2. Evaluate the Fréchet derivatives of the vertical magnetic field component $\partial\bar{B}_z/\partial\sigma_m$ in the wavenumber domain for a range of wavenumbers ky, by contour integration of the values of the electric potentials over the boundaries of the resistivity blocks;
3. Inverse Fourier Transform the $\partial\bar{B}_z/\partial\sigma_m$ magnetic field sensitivity from the wavenumber domain to the spatial domain.

Electric Potential Sensitivities

Following Park and Van (1991), sensitivity of the electric potential at any node in a finite element mesh to a change of the m^{th} resistivity block is reduced to the inner product of the current density **j** from a point source at the transmitter (Earth's surface) and the current density **j**´ from a unit point source at the required node, integrated over the perturbed volume:

$$\delta\phi(\mathbf{r}_p)=\int_{v_m}\delta\rho(\mathbf{r}')\mathbf{j}(\mathbf{r}_c,\mathbf{r}')\mathbf{j}'(\mathbf{r}_p,\mathbf{r}')dv', \tag{7}$$

where $\mathbf{r}_c$ and $\mathbf{r}_p$ are the position vectors of current and potential electrodes and v_m denotes the whole of the m^{th} perturbed block.

Accordingly, for a homogeneous half-space with resistivity ρ, the change in the potential $\delta\phi$ resulting from a change in the subsurface resistivity $\delta\rho$ may be written as:

$$\delta\phi(\mathbf{r}_p)=\frac{\delta\rho}{\rho^2}\int_{v_m}\nabla\phi_c(\mathbf{r}_c,\mathbf{r}')\nabla\phi_p(\mathbf{r}_p,\mathbf{r}')dv', \tag{8}$$

where ϕ_c and ϕ_p are potentials from a point source located at the transmitter and receiver respectively.

To calculate the partial derivatives for the TFMMR response, we require electric potential Fréchet derivatives in wavenumber domain for all mesh nodes. An analytical solution for calculating the Fréchet derivatives for all mesh nodes is developed here. The electrical potential distribution resulting from a current electrode located on the Earth's surface at origin $\mathbf{r}_c$ = (0, 0, 0) and a potential electrode located at the receiver point (node position) $\mathbf{r}_p = (x_p, y_p, z_p)$ is:

$$\phi_c(r)=\frac{\rho I}{2\pi r}, \text{ and} \tag{9}$$

$$\phi_p(\mathbf{r}_p,\mathbf{r})=\frac{\rho I}{2\pi|\mathbf{r}-\mathbf{r}_p|}+\frac{\rho I}{2\pi|\mathbf{r}-\mathbf{r}'_p|}, \tag{10}$$

in which $r = |\mathbf{r}|$ is the spatial distance from the origin, $\mathbf{r}_p$ is the position vector of the receiver, and $\mathbf{r}'_p$ is the position vector of the image of the receiver point (mesh nodes here) denoted by $\mathbf{r}'_p = (x_p, y_p, z'_p = -z_p)$, required to match the boundary conditions across the Earth's surface. The applied current is *I*, and ρ is the resistivity of the half-space.

Taking the inner product of the gradient of equations (9–10) and substituting in equation (8) results in:

$$\frac{\partial\phi(\mathbf{r}_p)}{\partial\rho_m}= \frac{I}{4\pi^2}\iiint_{v_m}\left[\frac{x(x-x_p)+y(y-y_p)+z(z-z_p)}{r^3((x-x_p)^2+(y-y_p)^2+(z-z_p)^2)^{3/2}}+\frac{x(x-x_p)+y(y-y_p)+z(z-z'_p)}{r^3((x-x_p)^2+(y-y_p)^2+(z-z'_p)^2)^{3/2}}\right]dxdydz, \tag{11}$$

For a 2D model striking in the y-direction, the limits of the integration along the y axis run from -∞ to +∞ :

$$\frac{\partial\phi(\mathbf{r}_p)}{\partial\rho_m}= \frac{I}{4\pi^2}\iint_{v_m}dxdz\int_{-\infty}^{\infty}\left[\frac{x(x-x_p)+y(y-y_p)+z(z-z_p)}{r^3((x-x_p)^2+(y-y_p)^2+(z-z_p)^2)^{3/2}}+\frac{x(x-x_p)+y(y-y_p)+z(z-z'_p)}{r^3((x-x_p)^2+(y-y_p)^2+(z-z'_p)^2)^{3/2}}\right]dy, \tag{12}$$

To obtain the corresponding expression in the wavenumber domain, we simply take the Fourier Transform of equation (12) and note that the integrand is a set of convolution integrals, offering the application of the Fourier Transformation of the convolution integrals as follows:

$$\frac{\partial\phi(\mathbf{r}_p,k_y)}{\partial\rho_m}=\frac{\partial\phi(x_p,k_y,z_p)}{\partial\rho_m}= \frac{Ik_y^2}{4\pi^2}\iint_{v_m}dxdz\left[\mathrm{K}_1(ak_y)\mathrm{K}_1(bk_y)\left(\frac{x_{cp}}{ab}+\frac{z_{cp}}{ab}\right)+\mathrm{K}_1(ak_y)\mathrm{K}_1(ck_y)\left(\frac{x_{cp}}{ac}+\frac{z'_{cp}}{ac}\right)+\mathrm{K}_0(ak_y)\mathrm{K}_0(bk_y)+\mathrm{K}_0(ak_y)\mathrm{K}_0(ck_y)\right], \tag{13}$$

in which the following notations have been used:

$$a = (x^2 + z^2)^{1/2} , \quad (14)$$

$$b = \left[(x - x_p)^2 + (z - z_p)^2\right]^{1/2} , \quad (15)$$

$$c = \left[(x - x_p)^2 + (z - z'_p)^2\right]^{1/2} , \quad (16)$$

$$x_{cp} = x(x - x_p) , \quad (17)$$

$$z_{cp} = z(z - z_p) , \quad (18)$$

$$z'_{cp} = z(z - z'_p) , \quad (19)$$

and K_0 and K_1 are zero- and first-order Bessel functions. The electric potential partial derivatives in equation (13) for all mesh nodes may be computed efficiently and accurately through a number of modified Bessel function evaluations, followed by numerical integration over all resistivity blocks ρ_m in the model.

Magnetic Field Sensitivities

Having obtained the partial derivatives of the electric potential with respect to each individual resistivity block we need then to evaluate the following integrals (from equation 5) for each data point:

$$I_1 = \frac{\mu_0}{2\pi}\int_0^\infty\int_{-\infty}^\infty k_y \left[\frac{\partial\bar{\phi}}{\partial\sigma_m}\sum_{m=1}^{M}\sigma_m\frac{\partial\psi_m(x',z')}{\partial x'}\right] K_0(k_y r')\, dx'dz' , \quad (20)$$

and

$$I_2 = \frac{\mu_0}{2\pi}\int_0^\infty\int_{-\infty}^\infty k_y \left[\bar{\phi}(x',z')\delta(\sigma(x',z') - \sigma_m)\frac{\partial\psi_m(x',z')}{\partial x'}\right] K_0(k_y r')dx'dz' . \quad (21)$$

Assuming a linear variation of transformed electric potential and its gradient over the boundary of the elements, we derive the discretised form of equations (20–21) as two summations given by:

$$I_1 = \frac{\mu_0}{2\pi} k_y \sum_{i=1}^{Nx}\sum_{j=1}^{Nz}\left[\frac{\bar{\phi}'_{i,j} + \bar{\phi}'_{i,j+1}}{2}(\sigma_{i,j} - \sigma_{i-1,j})\int_{z_j}^{z_{j+1}} K_0(k_y r'_i)\, dz' + \frac{\bar{\phi}'_{i+1,j} + \bar{\phi}'_{i+1,j+1}}{2}(\sigma_{i+1,j} - \sigma_{i,j})\int_{z_j}^{z_{j+1}} K_0(k_y r'_{i+1})\, dz'\right] , \quad (22)$$

and

$$I_2 = \frac{\mu_0}{2\pi} k_y \sum_{i=1}^{Nx}\sum_{j=1}^{Nz}\left[\frac{\bar{\phi}'_{i,j} + \bar{\phi}'_{i,j+1}}{2}\mathrm{Sgn}(\sigma_{i,j} - \sigma_k)\int_{z_j}^{z_{j+1}} K_0(k_y r_i)\, dz' + \frac{\bar{\phi}'_{i+1,j} + \bar{\phi}'_{i+1,j+1}}{2}\mathrm{Sgn}(\sigma_{i,j} - \sigma_k)\int_{z_j}^{z_{j+1}} K_0(k_y r_{i+1})\, dz'\right] , \quad (23)$$

where

$$\bar{\phi}'_{i,j} = \frac{\partial\bar{\phi}_{i,j}}{\partial\sigma_m} , \quad (24)$$

$$r'_i = \sqrt{(x - x_i)^2 + (z - z')^2} \quad \text{, and} \quad (25)$$

$$r'_{i+1} = \sqrt{(x - x_{i+1})^2 + (z - z')^2} . \quad (26)$$

N_x and N_z are the number of resistivity blocks in the x and z directions, respectively, and Sgn is the sign function defined as:

$$\mathrm{Sgn}(x) = \begin{cases} 1 & \text{when } x > 0 \\ 0 & \text{when } x = 0 \\ -1 & \text{when } x < 0 \end{cases} . \quad (27)$$

MARQUART-LEVENBERG INVERSION

The Marquart-Levenberg approach has been extensively discussed (e.g., Line and Treitel, 1984; Scales, 1985; Hohmann and Raiche, 1988). Here, we start with the ordinary least-squares equation, also known as the Gauss-Newton method, relating the parameter correction vector to the data-misfit via the first-order partial derivatives of the data with respect to each parameter in the matrix form:

$$\Delta\mathbf{P} = \left[\mathbf{J}^T\mathbf{J}\right]^{-1}\mathbf{J}^T\Delta\mathbf{D} , \quad (28)$$

where $\Delta\mathbf{P}$ is the parameter correction vector, $\mathbf{J}$ is the Jacobian matrix, $\Delta\mathbf{D} = \mathbf{d} - \mathbf{y}$ is the residual (difference between data ($\mathbf{d}$) and the current predicted response of the forward model ($\mathbf{y}$)), and T denotes the transpose of the matrix. For a total of M model parameters, and for the forward model evaluated at location n, the Fréchet derivative element of the Jacobian matrix is:

$$J_{mn} = \frac{\partial F_n}{\partial p_m} = \frac{\partial F_n(p_1,\ldots,p_M)}{\partial p_m} , \quad (29)$$

in which the function F represents the forward model.

Equation (28) involves the construction of the matrix $\mathbf{J}^T\mathbf{J}$ and its inverse. As $\mathbf{J}$ may be close to singular, a smoothness-constrained modification is used. A smoothness filter $\mathbf{C}$ stabilises both the inversion process and improves the condition of the Jacobian matrix (Tikhonov and Arsenin, 1977; Constable et al., 1987). This leads to the following system of normal equations:

$$\Delta\mathbf{P} = \left[\mathbf{J}^T\mathbf{J} + \beta\mathbf{C}^T\mathbf{C}\right]^{-1}\left[\mathbf{J}^T\Delta\mathbf{D}\right] , \quad (30)$$

in which β is the Marquardt, or damping, factor.

Sasaki (1989) and Loke and Barker (1996) note that the 2D smoothness filter $\mathbf{C}$ is used to constrain the smoothness of the perturbations to the model parameters to some constant value. The value of the damping factor β depends on the level of random noise present in the data; a larger value of β is used for higher level of noise. It is very important that a proper smoothness filter for a blocky parameterisation model is used in the entire course of inversion. Here, the smoothness filter proposed by Sasaki (1989) was adopted. The approximate size of the smoothness (or roughness) of the spatial variation in resistivity around each block is defined as

$$\delta\rho'_m = \delta\rho^L_m + \delta\rho^R_m - 4\delta\rho_m + \delta\rho^U_m + \delta\rho^L_m \quad \text{for m = 1,...,M} , \quad (31)$$

where superscripts L and R refer to blocks horizontally adjacent to the m^{th} block, and U and L are blocks above and below, and the δ symbol represents the change from the previous model parameter (Sasaki, 1989). Equation (31) can be written in a matrix form as:

$$\Delta\mathbf{P}' = \mathbf{C}\Delta\mathbf{P} \quad (32)$$

where $\mathbf{C}$ is a sparse ($M \times M$) matrix whose coefficients are either 1, -4, or 0.

In the Marquardt-Levenberg method, equation (30) is solved iteratively to improve the model fit to the data in a least-squares sense. The Fréchet derivatives in equation (29) are determined from equations (22–23) after inverse Fourier Transformation to the spatial domain. The smoothing filter $\mathbf{C}$ (which effectively couples together adjacent blocks) is easily determined from equation (32), and finally β is chosen a priori, based on knowledge of the noise levels in the observations.

QUASI-NEWTON APPROACH

In the case of TFMMR data and for a moderate number of parameters (say less than a few hundred) the most time consuming task is to recompute the Fréchet derivatives (equation 29) for each parameter set **P**. To reduce the time taken in computation, a quasi-Newton approach (Loke and Barker, 1996) was adopted. In the quasi-Newton approach we avoid the re-calculation of the Jacobian matrix by using an updating method. The Jacobian matrix $\mathbf{J}_{i+1}$ for the $(i+1)^{th}$ iteration is replaced by an approximation $\mathbf{A}_{i+1}$ using Broyden's recursive formula (Broyden, 1965; Loke and Barker, 1996):

$$\mathbf{A}_{i+1} = \mathbf{A}_i + \left[(\Delta \mathbf{y}_i - \mathbf{A}_i \Delta \mathbf{P}_i)/(\Delta \mathbf{P}_i^T \mathbf{P}_i)\right]\Delta \mathbf{P}^T \ , \qquad (33)$$

in which $\Delta \mathbf{y}_i$ is the discrepancy between the current and previous response of the forward solutions and $\mathbf{A}_i$ is the Jacobian matrix for the i^{th} iteration.

This updating formula is considered to be a rank-one quasi-Newton method (Scales, 1985; Loke and Barker, 1996). The number of arithmetic operations for this updating formula is proportion to N^2, where n is the number of data points. Thus, it is much faster than re-calculating the Jacobian matrix for electric potential derivatives of the measurement points (proportional to N^3). The only disadvantage of this approach is with a slower convergence compared to the case in which the Jacobian matrix is recalculated after every iteration.

Singular value decomposition was employed to solve the least-squares equation for the parameter correction vector in equation (30). Although the speed of such solution is slower than the Cholesky decomposition method, it is more robust, accurate, and less sensitive to the ill-conditioned problems where the Jacobian matrix is singular or nearly singular (Lines and Treitel, 1984). Furthermore, for small parameter number of less than one hundred, its performance is comparable with other methods.

FLYING DOCTOR DEPOSIT, BROKEN HILL

The Flying Doctor deposit is located 5 km north-east of Broken Hill, in the far western part of NSW, close to the South Australian border (Stevens et al., 1980; Bradley, 1984; Burton, 1994; Hill et al., 2003). The Pb-Ag-Zn mineralisation occurs within the Broken Hill Group, which consists of a variable sequence of metasedimentary gneisses, quartzo-feldspathic gneisses, pegmatites, amphibolites, iron formations, and the lode-horizon rocks. A layer of transported regolith cover up to 3 m thick blankets the entire area (Hill et al., 2003). The deposit was originally detected by induced polarization (IP) profiling as a zone of significant anomalies. Subsequent drilling delineated sub-economic reserves of 300 000 tonnes, averaging 5.7% Pb, 3% Zn, and 59g/t Ag. The deposit has become an important test site for evaluating new geophysical techniques (e.g., Boggs et al., 1998). Bishop (1989) has compiled an evaluation report on the applicability of various EM techniques, IP, magnetic induced polarization (MIP), gradient array resistivity, magnetics, and radiometrics.

TFMMR Survey

The survey over the Flying Doctor deposit was conducted using a typical TFMMR gradient array configuration shown in Figure 1. The survey area (4500E to 5100E and 20000N to 20600N) covered 600 m · 600 m, coincident with a previous feasibility trial TFMMR survey undertaken by Cattach (Cattach, 1996). The survey square had a local "grid north" orientated 50° east of geomagnetic north, and with a magnetic field inclination of -66°. A current dipole had a separation of 1400 m, oriented along the North-South grid-line at 4800E, with coordinates c_1 = (4800E, 19600N) and c_2 = (4800E, 21000m), delivering a 6 A current square wave with 50% duty cycle and 8 Hz fundamental frequency.

TFMMR data were collected on foot with an optically pumped magnetometer (TM-4; Stanley and Cattach, 1996), with average speed of 1.5 m/s in East-West orientations, and with a sampling interval of 0.5 m. The profile line interval was set to 50 m mainly to reduce the survey cost, thus yielding 13 lines of data. Average production rate per crew is of order 10 km/day, primarily due to the logistics of uploading data after a few line profiles.

In addition to the current dipole aligned along geological strike, two other current dipoles were investigated. With the same current dipole length of 1400 m, current dipoles were also set up to be (a) perpendicular to the geological strike, and (b) at 45º to geological strike. In both cases, TFMMR data were again collected along 50 m spaced lines orientated East-West in the same survey grid.

Data Reduction

To determine the anomalous TFMMR response we must distinguish between the major components of the total raw TFMMR signal to be able to remove the undesired components (Cattach et al., 1994). The total magnetic field measured by the SAM receiver is composed of two major spectrally-distinct components; (a) a spatially-varying magnetic field ($\mathbf{B}_s$); and (b) a temporally-varying low-frequency magnetic field ($\mathbf{B}_{mod}$) due to the transmitted signal. The total magnetic intensity B_T is then:

$$B_T = \left|\mathbf{B}_s + \mathbf{B}_{\text{mod}}\right| \ . \qquad (34)$$

The modulation part consists of a primary field ($\mathbf{B}_{primary}$) due to current flow in the wires supplying the source and sink electrodes, and a magnetic field due to the current flowing in subsurface structures that consists of a normal field ($\mathbf{B}_{normal}$) and an anomalous field ($\mathbf{B}_{anomalous}$).

The anomalous TFMMR response is defined by Cattach et al. (1994) as:

$$B_{\text{anomalous}} = \left|\mathbf{B}_{\text{mod}} - \mathbf{B}_{\text{primary}} - \mathbf{B}_{\text{normal}}\right| \qquad (35)$$

Primary Field

The current flowing in the cables produces a magnetic field that may be computed by the Biot-Savart law. For the case of an infinitely long cable, the primary field is given by:

$$|\mathbf{B}| = \frac{\mu_0 I}{2\pi r} \ , \qquad (36)$$

where r is the orthogonal distance from the wire to a point in the survey area, and **B** only has a vertical component at the Earth's surface. In practice, if the length of the cable is five times longer than the distance *r* then the resulting field is effectively the same as that due to an infinitely long cable. In practice, we add up the contributions from each of the three wire components in Figure 1.

Normal Magnetic Field

The normal magnetic field is the magnetic field due to a current electrode embedded on the surface of a homogeneous, isotropic half-space (Edwards, et al., 1978). This field has only horizontal components and have been evaluated by Edwards (1974) and Siegel (1974). Due to the governing symmetry, the normal field is the same as the magnetic field from a cable extending vertically-

downwards from Earth surface and carrying the same current as the electrode (Siegel, 1974). In Cartesian co-ordinates these components are:

$$B_x^n(x,y,0) = -\frac{\mu_0 I}{4\pi}\left(\frac{y}{x^2+y^2}\right), \quad (37)$$

$$B_y^n(x,y,0) = \frac{\mu_0 I}{4\pi}\left(\frac{x}{x^2+y^2}\right). \quad (38)$$

The normal TFMMR field is the component of the resultant normal field projected in the Earth's geomagnetic field:

$$\text{TFMMR}_{normal}(x,y,0) = B_x^n(x,y,0)\cos D\cos I + B_y^n(x,y,0)\cos D\sin I\ , \quad (39)$$

where D is the geomagnetic declination and I is the geomagnetic field inclination in the surveying area.

There are two important features of the normal TFMMR parameter that it is appropriate to mention. Firstly, unlike the normal B_x component, the normal TFMMR field is asymmetric in both x- and y-directions. Secondly, the polarity of the normal TFMMR field always changes in the y-direction since the normal B_y component is even with respect to the y-coordinates.

Equation (38) shows that the TFMMR field is approximately the original applied field projected in the direction of the geomagnetic field. Therefore, the TFMMR response derived from filtering the raw magnetic signal is approximately equal to one component of the anomalous magnetic field produced by subsurface anomalous current flow in the direction of the geomagnetic field. As a typical survey area rarely exceeds a few square km, direction of the regional geomagnetic field is constant over the surveying area, so that we may write:

$$\nabla^2(\text{TFMMR}) = \nabla^2(\hat{\mathbf{F}}\cdot\mathbf{A}) = \hat{\mathbf{F}}\cdot\nabla^2(\mathbf{A})\ , \quad (40)$$

where **A** is the applied field, which is small compared with the Earth's geomagnetic field **F**. It can be shown that a potential field is harmonic then any spatial derivative is also harmonic (Kellogg, 1929). Therefore, as the applied field **A** is a harmonic function in the upper-half space, then the TFMMR response is also harmonic (subject to the conditions of an invariant geomagnetic field direction and **A** << **F**). This means that TFMMR responses can be processed as for other types of potential field data (e.g., gravity), including upward and downward continuation, first and second derivative filtering and, importantly, reduction to the pole.

Figure 2 shows the anomalous TFMMR data (equation 34) collected for case of the current electrodes aligned with geological strike (as in Figure 1). A linear high-amplitude trend coincident with the mineralisation and the Globe Vauxhall Shear zone, extending North-South is clearly seen from this figure. Figure 3 shows representative data sections along two lines 20450 and 20600, which clearly indicates noise levels that can be obtained.

Aligning the source and sink current electrodes perpendicular to geological strike generates a much smaller TFMMR response. This was demonstrated in equation (1) in which the B_z response (which is the TFMMR response if the Earth's magnetic field was vertical) is dependent on the gradient of the conductivity in the x-direction ($\partial\sigma/\partial x$) for a 2D Earth with conductivity constant in the y-direction. Figures 4, 5, and 6 show contour plots of TFMMR responses for the case where the current electrodes are along strike (Figure 4, as for Figure 2), perpendicular to strike (Figure 5) and at 45º to strike (Figure 6). TFMMR responses in Figure 5 and 6 are not zero, indicating that the resistivity structure is not uniformly 2D, but are generally a factor of two smaller than in Figure 4, and showing less coherent structure across the survey area.

NUMERICAL FORWARD MODELLING OF THE FLYING DOCTOR DEPOSIT

To test the feasibility of the Flying Doctor deposit for 2.5D forward modelling (Fathianpour et al., 2005) and hence 2D inversion, a numerical forward model was first constructed from available drill-hole and petrophysical constraints (Figure 7). Resistivity values were inferred from available geological and geophysical information (Table 1). Host rocks are sillimanite and quartzitic gneiss with a large resistivity range of 200–2400 Ω.m

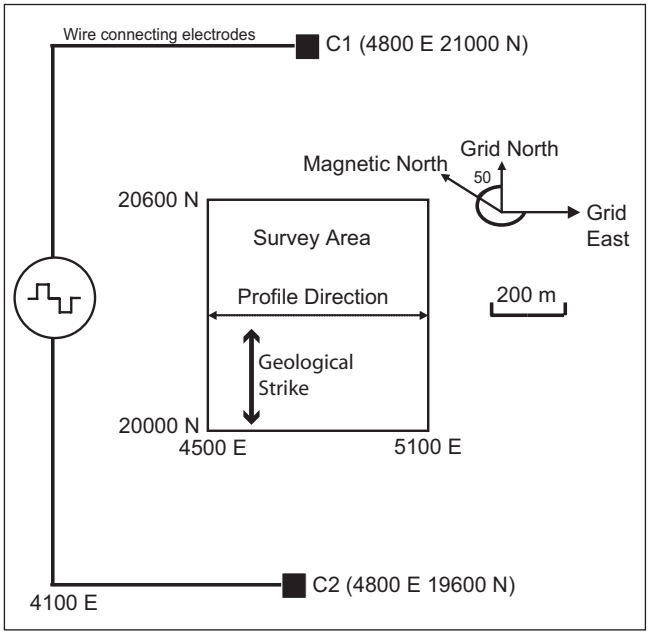

Fig. 1. TFMMR survey layout across the Flying Doctor Deposit. Current electrodes C1 and C2 are located along the direction of geological strike, and are separated by 1400 m.

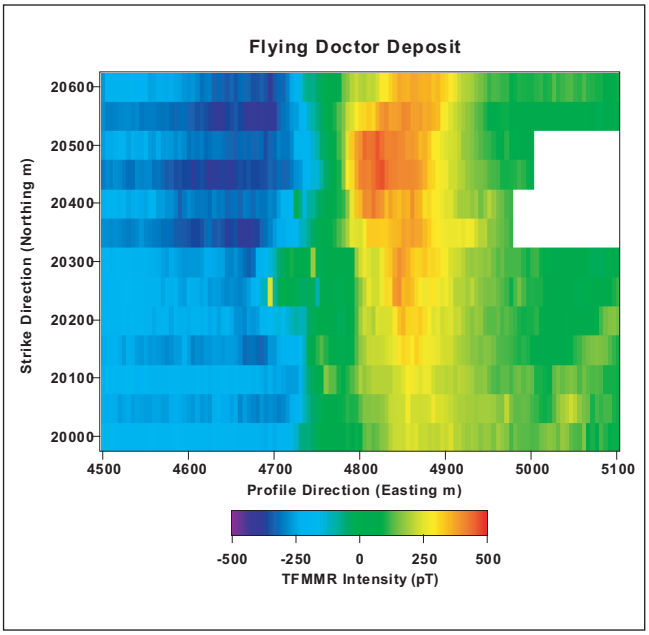

Fig. 2. TFMMR response collected for the survey layout in Figure 1. The plot shows raw data from 13 survey lines, each separated by 50 m over a grid area 600 m by 600 m.

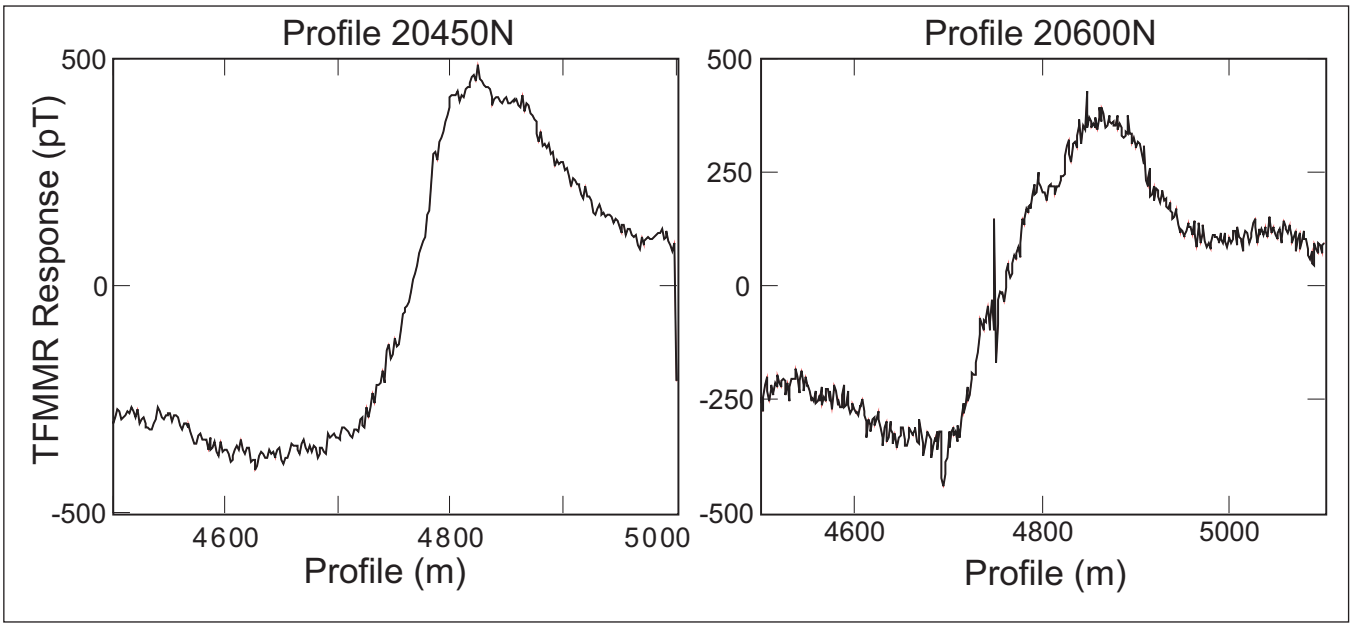

Fig. 3. Raw TFMMR data for profiles 20450N and 20600N across the survey area in Figure 1.

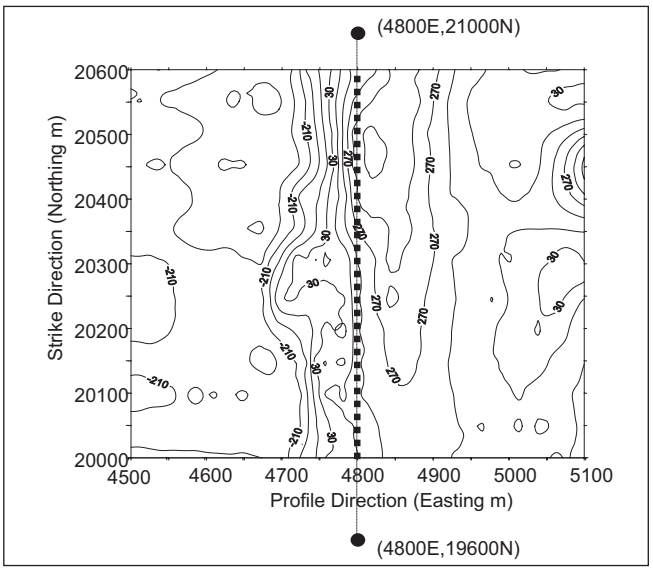

Fig. 4. Contour plot of the TFMMR response for the case in which current electrodes are located parallel to the strike of the mineralisation, 1400 m apart. Contour labels are in units of pT. The dashed line shows the approximate strike and surface projection of the mineralisation.

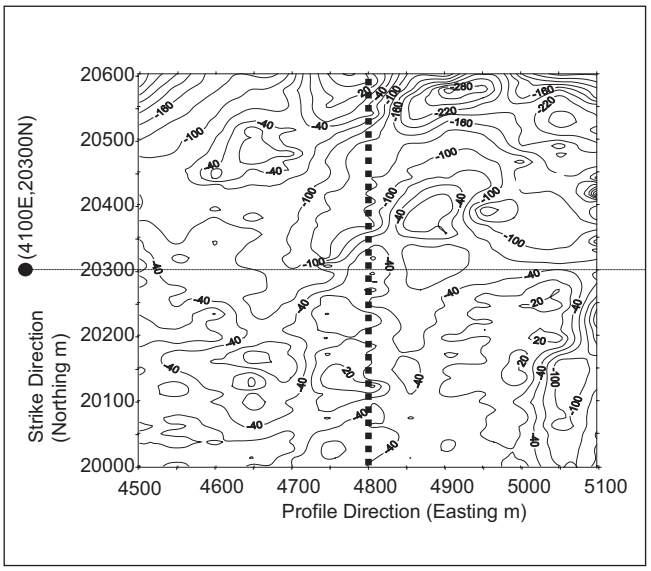

Fig. 5. Contour plot of the TFMMR response for the case in which current electrodes are located perpendicular to the strike of the mineralisation, 1400 m apart. Contour labels are in units of pT. The dashed line shows the approximate strike and surface projection of the mineralisation.

Rock Type	Resistivity range (Ω.m)	Resistivity used in modelling (Ω.m)	Reference
Psammite and Amphibolite	200–2000	1300	Emerson (1993)
Pelite	200–2000	2000	Emerson (1993)
Potosi Gneiss	200–2000	1300	Emerson (1993)
Shear Zone	1–200	180	Emerson (1993)
Mineralisation (50% ore, 50% Gangue)	0.75–130	-	Telford et al. (1990)
Low grade ore (10% ore, 90% Gangue)	-	90	Telford et al. (1990)

Table 1. The assigned resistivity values for the major rock units in the Flying Doctor deposit. The resistivities used for modelling were found from trial and error forward calculations to match the observations.

(Emerson, 1993). Resistivity of weathered metamorphic units associated with the mineralisation is very close to that of the ore bearing rock, with almost the same range of resistivities. The western part of the survey area is also highly sheared which results in decrease in resistivity value.

Although the sulphide mineralisation is generally tabular and dips steeply to the west, it exhibits a considerable variation both in depth and thickness in cross-sectional shape over the 450 m strike length between profiles 20000N to 20450N. However, for profiles in this range a 2.5D model is a good approximation as the length of the mineralisation in the strike direction is more than five times its thickness. The TFMMR response of the model is plotted with corresponding field data in Figure 8. In general the magnitude and shape of the anomalous TFMMR obtained through forward modelling is similar to that of the real field data for profile 20250N.

NUMERICAL INVERSION OF THE FLYING DOCTOR DEPOSIT DATA

The first step in the inversion was to pre-process observed TFMMR data with a reduction-to-the-pole algorithm, so that the TFMMR response was identical to the anomalous B_z component. The importance of this step is that Fréchet derivatives for only one magnetic field component are required, which simplifies the computational stages enormously. We have shown previously that the B_z component is primarily sensitive to lateral variations in resistivity structure.

Using a mesh comprising of 100 resistivity blocks, reduced-to-the-pole TFMMR data from three representative profiles (20100N, 20250N and 20450N) were inverted using the Marquardt-Levenberg algorithm with quasi-Newton updating of the Jacobian. Resulting resistivity sections are shown in Figure 9, with the data fits in Figure 10. In general, all inverted profiles show vertical conductive structures corresponding to the mineralisation and Globe Vauxhall Shear Zone (A in Figure 9), and the western shear zones (B in Figure 9). The resistive pelites separating shear zones are also clearly identified (C in Figure 9). There is little depth resolution, as noted before, due to the sensitivity of the TFMMR response to lateral gradients in resistivity.

CONCLUSION

The process of inverting TFMMR data is complicated, owing to the fact that it is dependent on vector components of magnetic field that have different Fréchet derivatives with respect to model resistivity parameters. The simplest way to overcome this problem is to apply the reduction-to-the-pole approach to observed TFMMR data so that we only require Fréchet derivatives for the vertical B_z anomalous magnetic field. We show that for a 2D resistivity structure, such derivatives are sensitive to lateral changes in resistivity, but have little depth resolution.

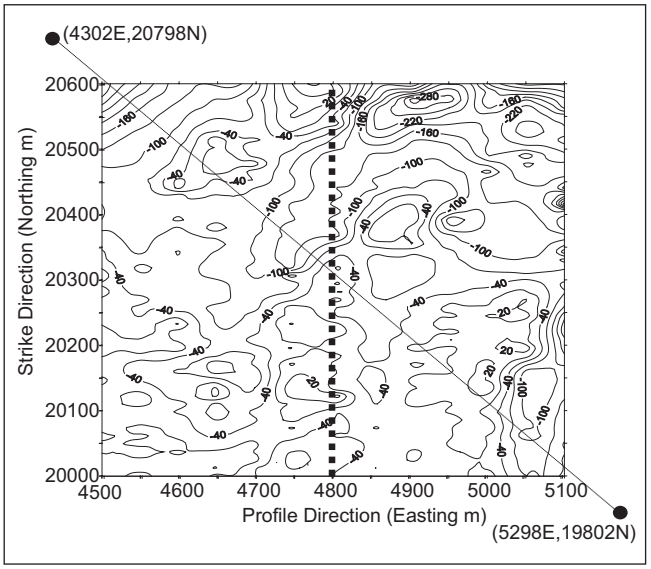

Fig. 6. Contour plot of the TFMMR response for the case in which current electrodes are located at an angle of 45° to the strike of the mineralisation, 1400 m apart. Contour labels are in units of pT. The dashed line shows the approximate strike and surface projection of the mineralisation.

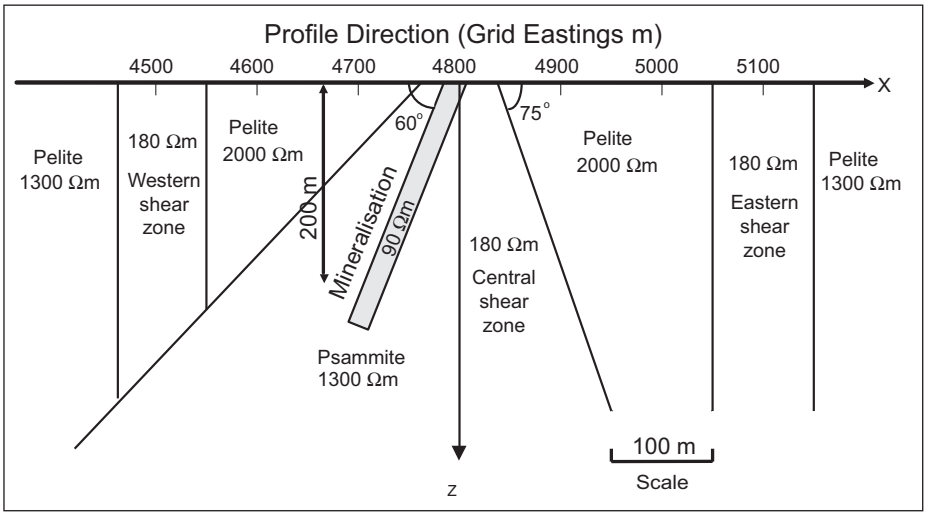

Fig. 7. Two-dimensional resistivity cross-section used in the construction of the numerical forward-model of profile 20250N. Model parameters were determined from drill hole intersections, and petrophysical measurements listed in Table 1.

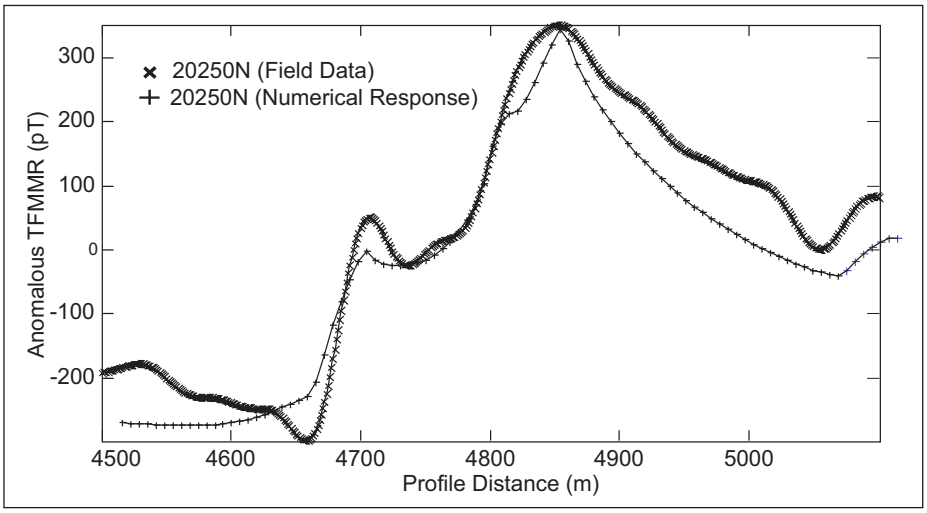

Fig. 8. A comparison between the observed TFMMR responses (after low-pass filtering) along profile 20250N collected with the survey layout in Figure 1, and the forward model response from the model shown in Figure 7.

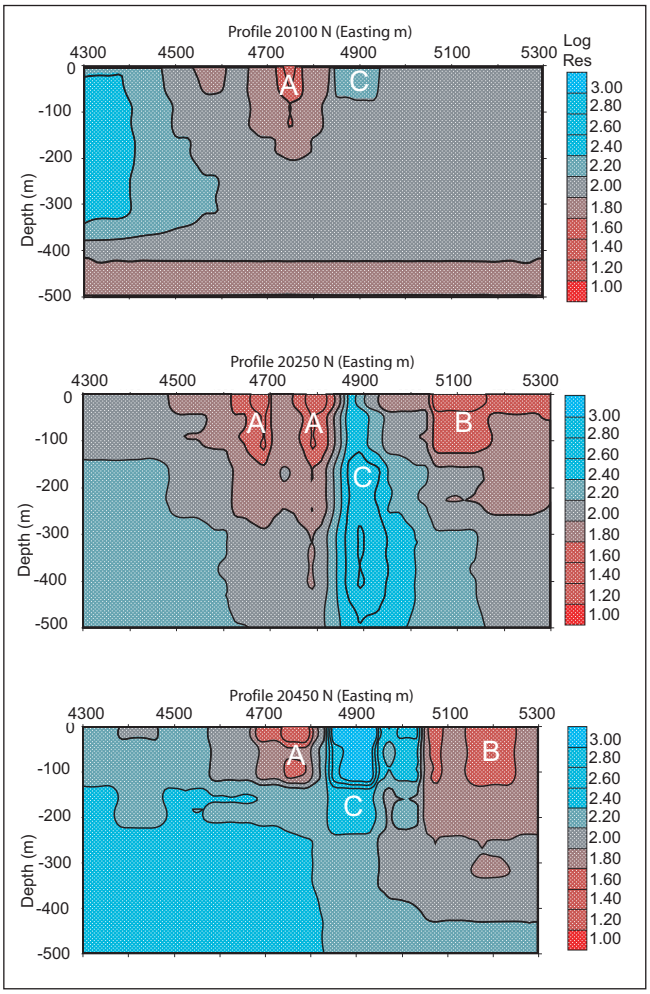

Fig. 9. Two-dimensional resistivity inversions of TFMMR data (reduced to the pole) from profiles 20100N, 20250N, and 20450N collected with the survey layout in Figure 1. The resistivity scale is in log units. The regions identified as "A" correspond to the mineralisation zone (4700–4800E) and the central shear zone (4800E) in Figure 7; the regions "B" are related to the eastern shear zone (at 5100 E); and "C" is the pelites separating the major shear zones.

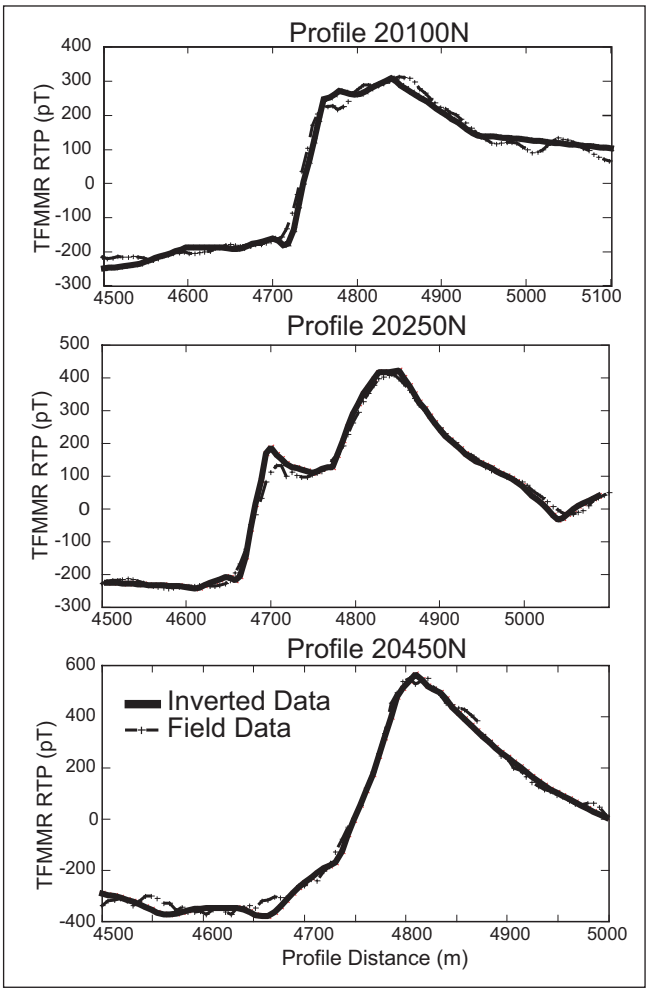

Fig. 10. A comparison between the observed TFMMR responses (reduced to the pole) along profiles 20100N, 20250N, and 2400N collected with the survey layout in Figure 1, and the inversions shown in Figure 9.

The Marquardt-Levenberg routine works well as an iterative inverse approach to minimising data misfit in a least-squares sense. However, as the Jacobian matrix of Fréchet derivatives can be close to singular, it is helpful to apply a smoothness constraint in a regularised inversion. There are various approaches to smoothness; we apply a simple formula that constrains changes in adjacent resistivity blocks through a simple filter, balanced by a damping factor β that can be pre-set to define the degree of smoothness (or roughness) required. The damping factor must be pre-set in our inversions (unlike the Occam inversion in which a line-search is applied at each iteration to find the optimum value of the Lagrange multiplier). A quasi-Newton updating formula was also used to approximate changes in the Jacobian matrix after each iteration, rather than re-calculating the Fréchet derivatives every time. For large numbers of model parameters, this is computationally efficient, although the rate of convergence is slightly slower.

Finally, we apply the modelling and inversion routines to TFMMR data collected across the Flying Doctor Deposit, near Broken Hill in New South Wales. Shear-zones hosting sub-economic mineralisation occur over several kilometres strike-length beneath a regolith cover, and hence is an ideal place to test the TFMMR method. We demonstrate that a strong TFMMR response can be obtained when current electrodes are separated 1400 m along the geological strike. However, when these current electrodes are placed in other orientations, but with the same offset, the TFMMR responses are smaller and are less laterally coherent.

Numerical 2.5D forward modelling of known structures using petrophysical measurements of resistivity as constraints corresponds well with observational data, giving confidence that TFMMR responses can be inverted for 2D resistivity structure. After applying the reduction-to-the-pole algorithm to reduce the anomalous component to just the vertical magnetic field B_z, numerical inversion for 2D resistivity structures of three lines of data clearly indicate zone of low resistivity in the basement. We have little depth sensitivity, but delineate lateral boundaries.

ACKNOWLEDGMENTS

We sincerely thank Dr John Stanley and Dr Malcolm Cattach for initial development of the research in the paper during Dr Nader Fathianpour's two-year postgraduate work at the University of New England. Mr David Boggs and colleagues at Geophysical Technology Limited are sincerely thanked for providing SAM equipment and assisting in field data collection in the Flying Doctor Deposit survey. At Flinders University, we acknowledge the

contributions of Professor S.A. Greenhalgh, Dr F.H. Chamalaun, Mr R. Eames and Mr A. Moradzadeh. Reviews of this paper by Associate Professor Jayson Meyers and Mr Stephen Griffin significantly improved the paper.

REFERENCES

Bishop, J.R., 1989, *An evaluation of geophysical test surveys over the Flying Doctor prospect: Broken Hill*: Report commissioned by Pasminco Mining Ltd.

Boggs, D.B., Stanley, J.M., and Cattach, M. K., 1998, Feasibility studies of TFMMIP and TFEM surveying with Sub-Audio Magnetics: *Exploration Geophysics*, **29**, 290–295.

Bradley, G.M., 1984, Mount Gipps 1:25,000 Geological Sheet 7234-III-S: *Geological Survey of NSW, Sydney*.

Broyden, C.G., 1965, A class of methods for solving non-linear simultaneous equations: *Mathematics of Computation*, 19, 577–593.

Broyden, C.G., 1972, Quasi-Newton methods: in Murray, W. (ed.), *Numerical Methods for Unconstrained optimisation*: Academic Press.

Burton, G.R., 1994, Metallogenic studies of the Broken Hill and Euriowie Blocks, New South Wales. 3. Mineral deposits of the South-Eastern Broken Hill Block: *Geological Survey of NSW, Bulletin,* **32** (3).

Cattach, M.K., Stanley, J.M., Lee, S.J., and Boyd, G.W., 1994, Sub-Audio Magnetics (SAM) – A high resolution technique for simultaneously mapping electrical and magnetic properties: *Exploration Geophysics*, **24**, 387–400.

Cattach, M.K., 1996, Sub-Audio Magnetic (SAM) - *A High Resolution Geophysical Method for Simultaneously Mapping Electrical and Magnetic Properties of the Earth*: Ph.D. thesis (unpublished), University of New England.

Constable, S.C., Parker, R.L., and Constable, C.G., 1987, Occam's inversion: A practical algorithm for generating smooth models from electromagnetic sounding data: *Geophysics*, **52**, 289–300.

Edwards, R.N., 1974, The magnetometric resistivity method and its application to the mapping of a fault: *Canadian Journal of Earth Sciences*, **11**, 1136–1156.

Edwards, R.N., Lee, H., and Nabighian, M.N., 1978, On the theory of magnetometric resistivity (MMR) method: *Geophysics*, **43**, 1176–1203.

Emerson, D., 1993, Petrophysics in exploration: *Preview*, **46**, 11–17.

Fathianpour, N., Heinson, G.S., and White, A., 2005, The total field magnetometric (TFMMR) method I: Theory and 2.5D forward modelling: *Exploration Geophysics*, (this volume).

Hill, S.M., Thomas, M., Earl, K.L., and Foster, K.A., 2003, Regolith expressions of mineralisation within the Flying Doctor Prospect, Northern Leases, Broken Hill, New South Wales. in Peljo, M.(Compiler), *Broken Hill Exploration Initiative: Geoscience Australia Record*, 81–82.

Hohmann, G.W., and Raiche, A.P., 1988, Inversion of controlled source electromagnetic data: in Nabighian, M.N. (ed.), *Electromagnetic Methods in Applied Geophysics*, **1**, 469–503: Society of Exploration Geophysicists.

Lines, L.R., and Treitel, S., 1984, Tutorial: A review of the Least-Squares inversion and its application to geophysical problems: *Geophysical Prospecting*, **32**, 159–186.

Loke, M.H., and Barker, R.D., 1995, Least-Squares deconvolution of apparent resistivity pseudosections, *Geophysics*, **60**, 1682–1690.

Kellogg, O.D., 1929, *Foundations of potential theory*: Springer.

McGillivray, P.R., and Oldenburg, D.W., 1990, Methods for calculating Fréchet derivatives and sensitivities for the non-linear inverse problem: A comparative study: *Geophysical Prospecting*, **38**, 499–524.

Park, S.K., and Van, G.P., 1991, Inversion of pole-pole data for 3-D resistivity structure beneath arrays of electrodes: *Geophysics*, **56**, 951–960.

Sasaki, Y., 1989, Two dimensional joint inversion of magnetotelluric and dipole-dipole resistivity data: *Geophysics*, **54**, 254–262.

Scales, L.E., 1985, *Introduction To Non-Linear Optimisation*: Springer-Verlag.

Siegel, H.O., 1974, The magnetic induced polarisation method: *Geophysics*, **39**, 321–339.

Stanley, J.M., and Cattach, M.K., 1990, The use of high definition mapping in engineering site investigation: *Exploration Geophysics*, **21**, 91–103.

Stevens, B.P.J., Stroud, W.J., Willis, I.L., Brown, R.E., Bradly, G.M., and Barnes, R.G., 1980, A stratigraphic interpretation of the Broken Hill block: in Stevens, B.P.J. (ed.), *Records of Geological Survey, NSW*, 9–32.

Telford, W.M., Geldart, L.P., and Sheriff, R.E., 1990, *Applied Geophysics*: Second Edition, Cambridge University Press.

Tikhonov, A.N., and Arsenin, V.Y., 1977, *Solutions of Ill-Posed Problems*: John Wiley & Sons.